6
Twist Grain Boundary Phases

Twist grain boundary (TGB) phases are frustrated phases, generally located between the cholesteric and the respective smectic phase. Like the Blue Phases, they can only be observed in chiral materials with large twisting power. In single component compounds their temperature region of phase existence is generally rather small, in the order of 1 K, while in mixtures the range of existence can sometimes be greatly enhanced. The TGBA* phase was theoretically predicted by Renn and Lubensky [1] in 1988, based on a formal analogy between the SmA phase and superconductors, as introduced by de Gennes [2]. In this analogy the twist grain boundary phase is the liquid crystal equivalent of the Abrikosov flux lattice phase of a type II superconductor in an external magnetic field [1, 3].

Although not being related to the textures of these phases, let us briefly outline this analogy. Consider a type I superconductor in its normal conducting (metal) phase at elevated temperatures. In this phase the magnetic induction lines of a relatively weak applied magnetic field will completely penetrate the material. Cooling into the superconducting state will result in an expulsion of the magnetic flux lines from the material, which is called the Meissner effect [4]. In a type II superconductor at a temperature below the conductor–superconductor transition, the material behaves like type I up to a certain critical field. Further increase of the magnetic field strength will result in a state where an incomplete Meissner effect is observed, with magnetic flux lines partially penetrating the material [5]. In this state, called the Abrikosov phase, flux lattice phase or vortex state, the superconducting properties are decreased. The distance to which the magnetic field can penetrate the superconducting material is called the London penetration depth [6]. The de Gennes analogy [2] treats the case of a second order nematic to SmA transition. In the analogy, a twist penetrates the SmA structure via a lattice of screw dislocations, just as the magnetic flux lines penetrate a type II superconductor via a lattice of vortices. In this case the nematic phase corresponds to a normal metal and the SmA phase to the Meissner phase of the superconductor. Thus twist expulsion in the liquid crystal is the analog to the Meissner effect. The de Gennes analogy was extended to chiral systems by Renn and Lubensky [1], i. e. to the N*–SmA* transition. Here the cholesteric phase corresponds to the conducting phase (normal metal) in a magnetic field, and thus the twist is the equivalent to the magnetic

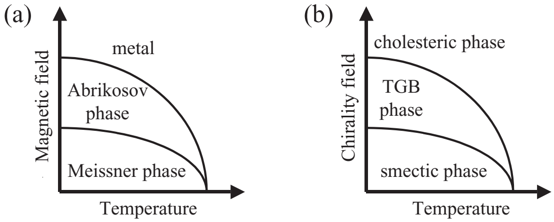

Fig. 6.1. Schematic phase diagram of (a) a type II superconductor in an applied magnetic field and (b) a chiral liquid crystal, illustrating the analogy of the Abrikosov flux lattice phase and the twist grain boundary TGBA* phase.

Tab. 6.1. Summary of some key quantities in the analogy between liquid crystals and superconductors.

Liquid crystal	***Superconductor***
nematic phase	normal metal
SmA phase	Meissner phase
cholesteric phase	normal metal in a magnetic field
nematic director, $\mathbf{n}$	magnetic vector potential, $\mathbf{A}$
"chirality field", $h = k_{22}q_0$	magnetic field, $\mathbf{H}$
twist, $q_0 = \mathbf{n}\ (\nabla \times \mathbf{n})$	magnetic induction, $\mathbf{B} = \nabla \times \mathbf{A}$
elastic energy	magnetic energy
screw dislocation	magnetic vortex (magnetic flux tube)
TGB phase	Abrikosov phase

induction in the case of superconductors. The twist penetration depth takes the role of the London penetration depth of the type II superconducting material. Associating the formed screw dislocations of the liquid crystal material with a vortex or magnetic flux tube of the superconductor, we arrive at the analogy of the TGBA* phase with the Abrikosov phase. This formal analogy is illustrated by the respective phase diagrams of both the type II superconducting material and the liquid crystal (Fig. 6.1) and is summarized in Tab. 6.1 [7].

After this brief excursion, let us now return to the structure and textures of twist grain boundary phases. TGB phases exhibit three basic key structural features:

- layered structure,
- helical superstructure,
- helix axis parallel to the smectic layer plane.

The TGB helix axis is thus perpendicular to the local director, which illustrates the close relationship between twist grain boundary phases and the high temperature cholesteric phase. The first experimental observation of a twist grain boundary phase was reported by Goodby et al. [8, 9], one year after its theoretical prediction.

6.1
The TGBA* Phase

As we have pointed out on several occasions above (Chapter 3), a twist such as observed in the cholesteric phase is for elastic reasons in general not compatible with the layered structure of the smectic A* phase. If on the other hand the tendency to helical superstructure formation is very strong, the competition between twist formation and smectic layer formation can result in a defect stabilized, frustrated structure, as shown in Fig. 6.2. Grains with a local SmA* layer structure are separated by regular arrays of screw dislocations, which can be realized by splay deformations in the director field and whose direction is parallel to the Burgers vector. These form the grain boundaries between adjacent grains (Fig. 6.3). The parallel screw dislocations of a single grain boundary are rotated by an angle $\Delta\alpha$ with respect to those of the adjacent grain, thus forming a helical superstruc-

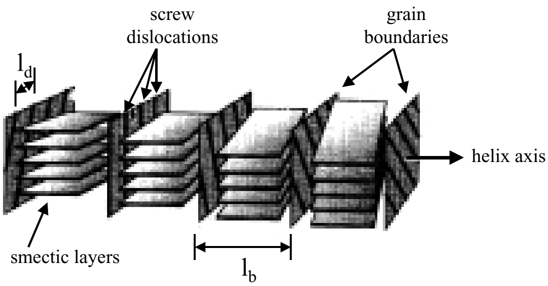

Fig. 6.2. Model structure of the twist grain boundary TGBA* phase.

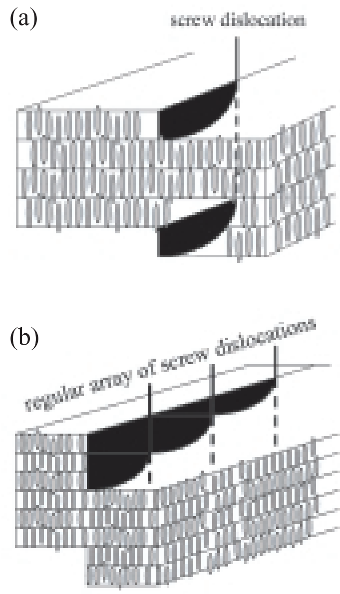

Fig. 6.3. Model structure of (a) a single screw dislocation and (b) a regular array of screw dislocations separating consecutive SmA* slabs of the TGBA* phase.

ture with twist axis perpendicular to the directors of each individual grain. This arrangement is quite similar to the structure of the N* phase and has directly been demonstrated by freeze–fracture transmission electron microscopy (TEM) studies [10].

The basic structural parameters of the TGBA* phase are the smectic layer thickness l, the helical pitch P, the thickness of smectic layer blocks l_b, i. e. the distance between adjacent grain boundaries, the distance between dislocation lines within a grain boundary l_d, and the twist between consecutive blocks $\Delta\alpha$ (see Figs. 6.2 and 6.3). From geometric considerations these parameters are related by the following relationships:

$$\Delta\alpha \approx l/l_\mathrm{d} \tag{6.1}$$

and

$$\Delta\alpha = 2\pi l_\mathrm{b}/P \tag{6.2}$$

(see Fig. 6.2). Combination of Eqs. (6.1) and (6.2) gives

$$P = 2\pi l_\mathrm{b} l_\mathrm{d}/\mathrm{r}l \tag{6.3}$$

From the x-ray investigations of Navailles et al. [11] (on a TGBC* phase), we can estimate the order of magnitude of the distance between screw dislocations by taking the grain block thickness to be in the order of $l_b \approx 1000$ Å and the pitch to be $P \approx 2$ μm. This yields a ratio of $l_d/l \approx 3$ or $l_d \approx 100$ Å. So far, x-ray investigations indicate that the structure of the TGBA* phase is often incommensurate [12–14], i. e. $360°/\Delta\alpha$ is an irrational number. This means that we do not have an integer number of grain blocks along a 2π twist (Fig. 6.4(b)). Recently however, also an example of a commensurate TGBA* phase has been reported [15] (Fig. 6.4(a)).

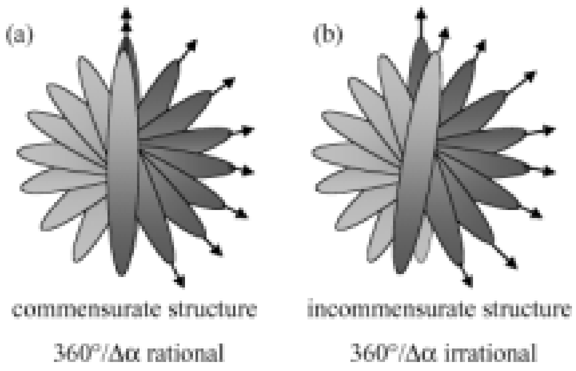

Fig. 6.4. Schematic illustration of (a) a commensurate and (b) an incommensurate structure of the TGBA* phase. An incommensurate structure is observed when it is formed by an irrational number of smectic slabs, while a commensurate structure consists of a rational number of smectic A* blocks within one pitch turn of the TGB helix.

6.1.1
Natural Textures

Owing to the often narrow temperature range of existence it is sometimes hard to detect the TGBA* phase not only by differential scanning calorimetry, but also by polarizing microscopy and texture observation. One method that can help to verify a twist grain boundary phase is the application of a temperature gradient across the sample, which results in a texture showing all three phases involved simultaneously, as shown in Plate 36 [16]. The temperature gradient is along the short edge of the texture photograph, exhibiting the SmA* fan-shaped texture at lower temperature at the top and the N* oily streaks texture at higher temperatures at the bottom of the image. In the middle part one can clearly detect the two phase boundaries separating the TGBA* phase.

Even for a larger temperature range of TGBA* phase existence it can sometimes not very easily be detected from natural textures with quasi-planar surface anchoring. Often the transition is only characterized by a smearing out of the high temperature phase texture, which in the case of a cholesteric oily streaks texture can be observed by the transformation of the sharp oily streaks defects into a slightly blurred structure (Plate 37). This texture cannot be clearly focused in the polarizing microscope. A similar appearance can also be observed when the TGBA* phase adopts a fan-like texture. An example is shown in Plates 38 and 39 on cooling. In Plate 38 the TGBA* phase is seen, appearing as a blurred fan-shaped texture, which cannot be clearly focused. Cooling across the TGBA* to SmA* transition one can observe a sudden sharpening of the fans, as seen in Plate 39. The discussed behavior can also be seen in Plate 36 on both sides of the phase boundaries, i.e. the N*–TGBA* transitions with a blurred Grandjean texture region and the TGBA*–SmA* transition with a blurred fan-shaped region.

For relatively thick samples, prepared between untreated glass plates, the TGBA* phase exhibits a quite unoriented appearance and can thus often be distinguished from the cholesteric and the SmA* phase. The series of texture photographs of Plates 40–42 [14] across the N*–TGBA*–SmA* temperature region illustrates this behavior.

6.1.2
Textures for Planar Anchoring Conditions

Subjecting the TGBA* phase to planar boundary conditions orients the molecular long axis parallel to the substrate and thus the smectic layer planes perpendicular to the glass plates. This implies that the TGBA* helix axis is oriented perpendicular to the substrate planes, similar to the Grandjean orientation of the cholesteric phase. The resulting structure is schematically depicted in Fig. 6.5, with an integer number of π twists fitting into the fixed cell gap. A typical texture of this arrangement is shown in Plate 43 [16] for a TGBA* phase with a pitch of several micrometers, confined to a cell gap of $d = 8$ µm and in Plate 44 for

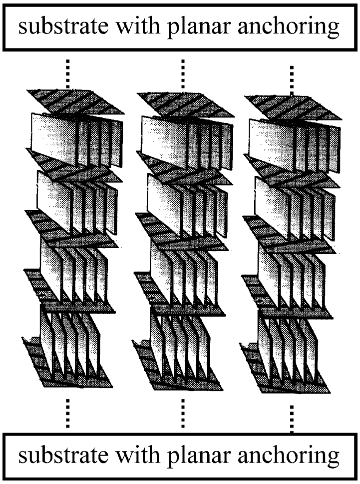

Fig. 6.5. Schematic illustration of a TGBA* phase confined to a cell with planar boundary conditions. TGB Grandjean steps may be observed whenever the pitch of the helical superstructure is changed by a π twist.

a short pitch material. The texture photographs were taken on cooling, with different colors corresponding to different twist states, due to the temperature dependence of the TGBA* pitch in the vicinity of the transition to SmA*. Rotation of the TGBA* phase maintaining the helix axis parallel to the direction of light propagation does not result in an extinction position between crossed polarizers, which is indicative of a helical superstructure. If the bounding substrates are not parallel to each other, the formation of TGBA* Grandjean steps is observed, resulting from half-pitch variations, i. e. changes of consecutive π twists. A corresponding texture is shown in Plate 45, which once again illustrates the close relationship between the TGBA* appearance and that of the cholesteric phase (compare to Plate 26).

6.1.3
Textures for Homeotropic Anchoring Conditions

If the TGBA* phase is subjected to homeotropic boundary conditions, the molecules orient with their long molecular axes perpendicular to the substrates, which results in an arrangement where the helix axis is lying in the plane of the bounding glass plates. Within the substrate plane the helix axis does not exhibit any preferred direction, just as discussed above for the N* phase. The resulting image observed between crossed polarizers is the so-called filament texture, an example of which is shown in Plate 46 at the transition from N* (left) to TGBA* (right) and in Plate 47 for the transition from SmA* (black) to TGBA* (filaments). For a sample with a long pitch TGBA* phase an equidistant pattern of dark lines is observed, which results from the helical orientation of the director, with a dark line appearing whenever the local director is oriented along the direction of light propagation (Plates 48 and 49). The periodicity L of the TGBA* phase is equal to half the pitch, so that the pitch can be estimated from $P = 2L$. The corresponding cell

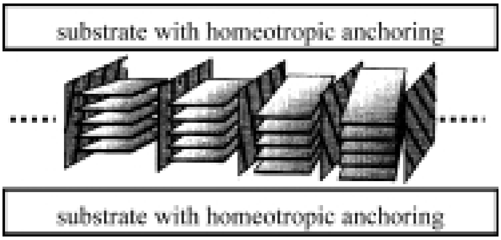

Fig. 6.6. Schematic illustration of a TGBA* phase confined to a cell with homeotropic anchoring conditions. For a sample where the pitch can be resolved by optical microscopy, *P* is given by twice the identity period, i. e. the distance between two adjacent dark lines of the equidistant line pattern corresponds to half the value of the TGB pitch.

configuration is schematically depicted in Fig. 6.6. At the transition to the SmA* phase the texture changes to the pseudo-isotropic texture, which is illustrated by the dark sample region at the top left of Plate 50.

6.1.4 Wedge Cell Preparations

Preparation of a sample in a wedge cell geometry under a temperature gradient is quite illustrative with respect to structural similarities and differences of N*, TGBA*, and SmA* textures [16]. Let us first consider the case of planar anchoring conditions, for which the respective texture photograph is shown in Plate 51, with the temperature gradient applied from right to left. At the low temperature side (right) the SmA* phase is observed with the director in the plane of the substrate. This part of the texture can be brought into an extinction position, when the optic axis is oriented along one of the polarizer directions. In the middle part of the texture the TGBA* is formed, which shows Grandjean steps. The TGBA* region cannot be brought to extinction. This indicates that the helical superstructure is oriented with the twist axis along the direction of light propagation, and different twist states are observed due to the wedge cell geometry. In the left part of the texture, the high temperature cholesteric phase can be seen with its typical oily streaks. Also here, the optic axis points along the direction of light propagation and no intensity change is observed by rotation between crossed polarizers. Fig. 6.7 schematically depicts the sample configuration discussed [16].

In a second preparation we subject the same sample to homeotropic boundary conditions. The respective texture photograph is shown in Plate 52 [16]. The low temperature SmA* phase on the right side is dark for all orientations of the sample between crossed polarizers, i. e. the optic axis is oriented parallel to the direction of light propagation. At the transition region into the TGBA* phase in the middle part of the texture, the typical filaments are observed, while at somewhat higher temperatures the TGBA* phase adopts a fan-like texture. The helix axis in this part is basically oriented in the substrate plane. The high temperature N* phase also exhibits a fan-like texture, but can easily be distinguished from the TGBA* phase by the change in birefringence. The respective sample configuration is schematically summarized in Fig. 6.8 [16].

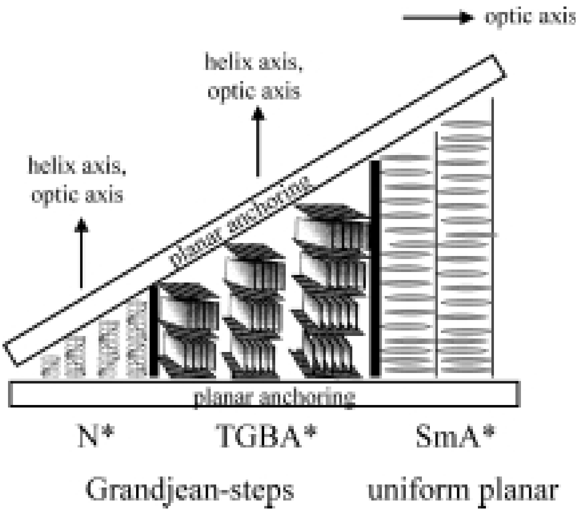

Fig. 6.7. Schematic illustration of a wedge cell preparation with planar boundary conditions of a sample with an N*–TGBA*–SmA* phase sequence under a temperature gradient. Corresponding to the texture photograph of Plate 51, the SmA* phase at the right part of the figure exhibits a director oriented in the plane of the substrate; the sample can be brought to extinction when the optic axis is oriented along one of the polarizer directions. The TGBA* phase in the middle of the figure exhibits a twist axis along the direction of light propagation; it thus shows a director configuration that cannot be rotated into an extinction position. Discontinuous Grandjean steps are observed due to the temperature dependence of the TGBA* pitch. In the left part of the figure the cholesteric phase is shown with its helix axis parallel to the incident light beam.

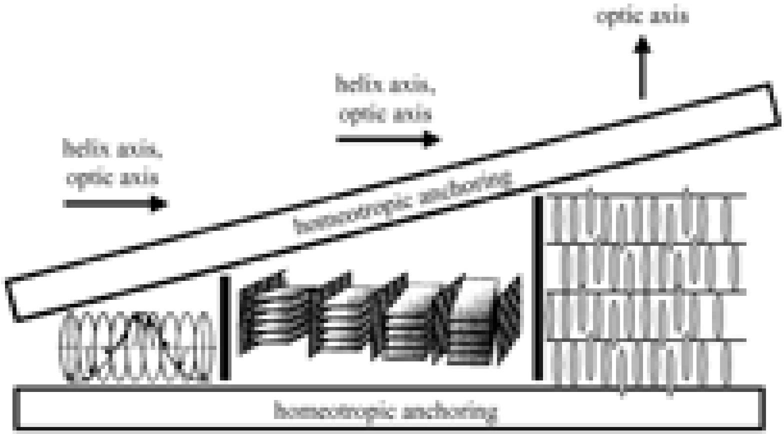

Fig. 6.8. Schematic illustration of a homeotropic boundary condition wedge cell preparation of a sample with an N*–TGBA*–SmA* phase sequence under a temperature gradient. Corresponding to the texture photograph of Plate 52, the pseudo-isotropic director configuration of the SmA* phase is illustrated at the right of the figure. In the center part the director orientation of the fan-like and filament TGBA* texture is illustrated, while the left part of the figure depicts the N* director orientation.

6.1.5
Droplet Preparation

The helix axis orientation of the TGBA* phase in comparison to that of the cholesteric and the SmC* phase can be nicely demonstrated by the observation of a droplet [17]. The sample with a phase sequence N*–TGBA*–SmC* is prepared as a droplet with an approximate diameter of 500 μm with a coverslip very gently placed on top. The sequence of Plates 53–55 shows the textures of the N*, TGBA*, and SmC* phases, respectively. In Plate 53 it can be seen that the cholesteric helix axis is basically oriented in the plane of the substrate, but without any preferred in-plane direction. Cooling the sample into the TGBA* phase the formation of a radially symmetric stripe pattern can be observed (Plate 54). This results from smectic layers being formed in a concentric fashion, with the TGBA* helix axis along the smectic layer planes and perpendicular to the long molecular axis. A schematic illustration of this arrangement is depicted in Fig. 6.9 [16]. Further cooling leads to the formation of the SmC* phase, which is shown in Plate 55. This is accompanied by a turn of the helical superstructure by 90°, because in SmC* the helix axis is oriented perpendicular to the smectic layer plane. In a droplet preparation with a concentric arrangement of smectic layers, the helix axis adopts a radial configuration and we thus observe a concentric pattern of equidistant lines due to the SmC* helical superstructure (see also Chapter 7). The corresponding schematic illustration is depicted in Fig. 6.10 [16].

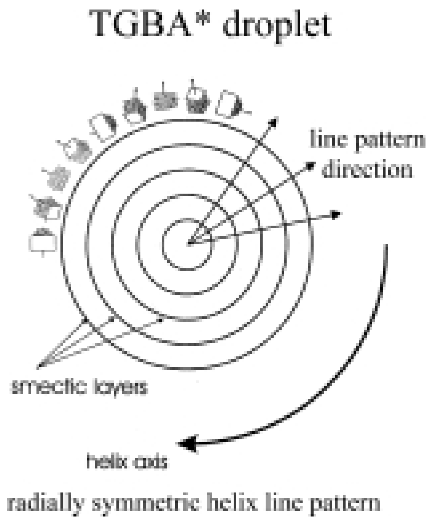

Fig. 6.9. Schematic illustration of the smectic layer orientation and TGBA* helix axis configuration in a droplet preparation with planar anchoring conditions. The TGBA* phase exhibits a helix axis that is oriented parallel to the smectic layer planes, resulting in a line pattern of radial symmetry. (Reproduced by permission of Taylor & Francis, I. Dierking, S. T. Lagerwall, *Liq. Cryst.*, **26**, (1999), 83 ⟨http://www.tandf.co.uk/journals⟩.)

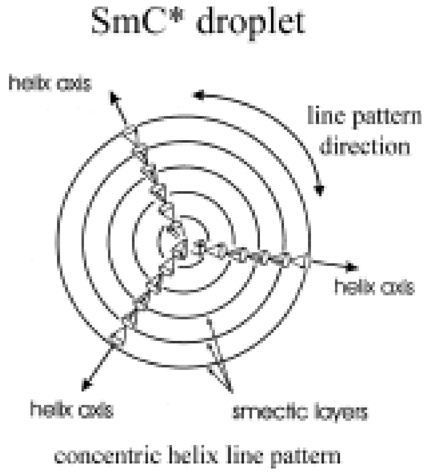

Fig. 6.10. Schematic illustration of the smectic layer orientation and SmC* helix axis configuration in a droplet preparation with planar anchoring conditions. The smectic C* helix axis is oriented perpendicular to the smectic layer plane, observable as a line pattern of equidistant concentric rings parallel to the smectic layer planes. (Reproduced by permission of Taylor & Francis, I. Dierking, S. T. Lagerwall, *Liq. Cryst.*, **26**, (1999), 83 ⟨http://www.tandf.co.uk/journals⟩.)

6.1.6
Suppression of the TGBA* Structure

Confining a TGB material to rather thin cell gaps, as compared to the pitch of its helical superstructure, can result in the suppression of the twist structure, due to a competition between elasticity and helix formation [17–19]. Let us again consider the sample discussed in the previous subsection, which exhibits an N*–TGBA*–SmC* phase sequence. Observation of the compound in a 4 μm cell with monostable planar boundary conditions clearly shows that the helical superstructure of the TGBA* phase is unwound and only the structure of the constituent smectic slabs remains. This is demonstrated in Plate 56 [16], which shows a typical uniform planar SmA* texture (right part of the photograph), which is here rotated out of the direction of the polarizers, but can be brought to extinction. This SmA* phase is transforming into SmC* (left part), which can be seen by the partial formation of helix lines. The phase sequence in thin cells is now N*–SmA*–SmC*, but it is emphasized again that the *bulk sample* does not exhibit an SmA* but rather a TGBA* phase (see droplet preparation in Plates 53–55).

6.2
The TGBC* Phases

While the structure and textures of the TGBA* phase seem to be quite well understood, these are to some extent still the subject of controversial discussion for the TGBC* phases. The possible occurrence of a TGBC* phase was theoretically predicted by Renn and Lubensky [3, 20], and again experimental evidence was provided soon after its prediction, this time by Nguyen and coworkers [21]. Owing to the local SmC* tilt of the molecules with respect to the smectic layer normal and to the existence of a spontaneous polarization, several different structures may in principle occur in the TGBC* phase [20]. Generally, the SmC* phase exhibits a helical superstructure in bulk samples (see Chapter 7). For several possible TGBC* structures this twist is expelled into the twist grain boundaries, which means that the local smectic C* slabs exhibit a uniform tilted director configuration. Concerning the nomenclature, there seems to be no agreement on how to name the different possible TGBC* structures. For this reason we will here refer to some of the proposed designations and schematic figures of the respective phases.

One possible configuration is schematically depicted in Fig. 6.11, which we will here call $TGBC_1$* and which is referred to as TGB_C in the notation of Luk'yanchuk [22]. Like in the TGBA* phase the smectic layer normal is perpendicular to the macroscopic twist axis, but the local director **n** is oriented under the molecular tilt angle θ with respect to the layer normal **k**. The vector of the spontaneous polarization $\mathbf{P}_S$ lies in the smectic layer plane and is perpendicular to the helix axis. Variation of the direction of the spontaneous polarization from slab to slab results in a macroscopic compensation of $\mathbf{P}_S$, and the phase would thus be helielectric, similar to SmC*.

A second possible structure is shown in Fig. 6.12 and is here referred to as $TGBC_2$*, corresponding to TGB_{Cp} in Ref. [22]. In this structure the director **n** is oriented along the direction of the screw dislocations and perpendicular to the helix axis. This implies that the smectic layer planes are tilted with respect to

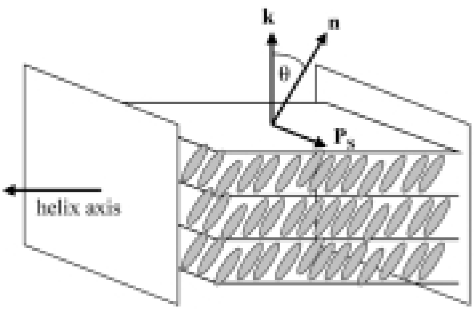

Fig. 6.11. Schematic model of the discussed $TGBC_1$* structure. The smectic layer normal **k** is perpendicular to the twist axis and the director **n** tilted with respect to the direction of screw dislocations. $\mathbf{P}_S$ spirals around the twist axis and macroscopically vanishes. The structure is helielectric.

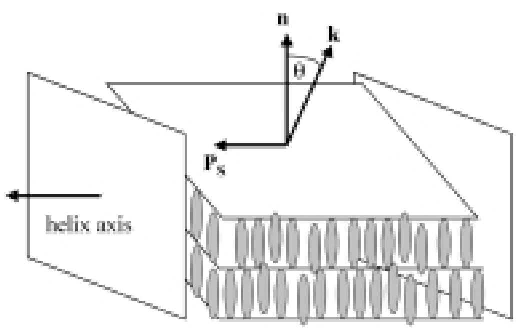

Fig. 6.12. Schematic model of the discussed $TGBC_2$* structure. The smectic layer normal **k** is tilted with respect to the direction of screw dislocations, while the director is parallel to them. The spontaneous polarization in all smectic slabs points along the helix axis. The structure is ferroelectric.

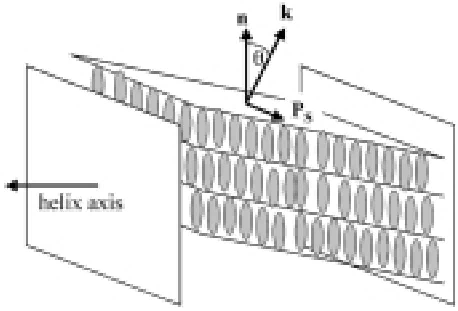

Fig. 6.13. Schematic model of the discussed $TGBC_3$* structure, which is in accordance with the x-ray investigations of Navailles et al. [11, 25]. The smectic layer planes are tilted with respect to the grain boundaries and the director **n** is parallel to the direction of the screw dislocations. The polarization vector spirals around the twist direction and the structure is helielectric.

the local director and the layer normal **k** makes an angle θ with the direction of the screw dislocations. The vectors of the spontaneous polarization of all smectic slabs point along the helix axis, and the phase would thus be truly ferroelectric.

Yet another possible TGBC* structure was proposed by Dozov et al. [23, 24] and is schematically depicted in Fig. 6.13. This will here be referred to as $TGBC_3$* and was named TGB_{Ct} in Ref. [22] and melted grain boundary (MGB) phase in Refs. [23, 24], indicating a vanishing smectic order parameter at the grain boundaries. The structure shows a director **n** parallel to the screw dislocations and a layer normal **k** that is inclined by the tilt angle θ with respect to the grain boundary plane. The vector of the spontaneous polarization is perpendicular to the helix axis and spirals around it as we proceed in direction of the twist axis, leading to a macroscopic compensation of $\mathbf{P}_S$ and thus to a helielectric phase. The synchrotron x-ray investigations performed by Navailles et al. [11, 25] on oriented samples indicate that the $TGBC_3$* is in fact the one generally observed. In contrast to the TGBA* phase the $TGBC_3$* phase generally seems to exhibit a commensurate structure [11, 25].

The textures of the $TGBC_3$* phase are analogous to those observed for TGBA*: Grandjean textures for planar boundary conditions and fingerprint/filament textures for homeotropic anchoring. One way to distinguish between the two phases may be the application of an electric field along the twist axis, while slowly increasing its amplitude. In TGBA* an electroclinic-like response should be observed [26, 27] and result in an unwound SmA* state at large field amplitudes [28]. The coupling between **E** and $\mathbf{P}_S$ in $TGBC_3$* should on the other hand distort the helical superstructure until unwinding [29] and lead to the observation of a ferroelectric response [30].

There is however another variant of a TGBC* phase, which can easily be recognized and has become known as the *square grid* texture [31, 32], depicted in Plate 57 for planar anchoring conditions [33]. There seems to be good evidence that the square grid pattern is in fact due to a TGBC* structure predicted by Renn [20]. In this case not only the occurrence of a helical superstructure due to the TGB helix is observed, but also the SmC* slabs exhibit the director helix of the bulk SmC* phase, with the helix axis perpendicular to that of the TGB twist. Following the suggestion of Kuczynski and Stegemeyer [31, 32] we will refer to this phase as

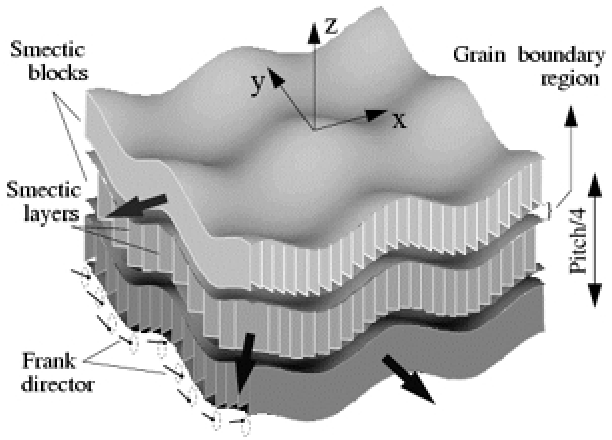

Fig. 6.14. Model structure of the UTGBC* phase to explain the *square grid* texture. (Reproduced by permission of Taylor & Francis, P. A. Pramod et al., *Liq. Cryst.*, **28**, (2001), 525 ⟨http://www.tandf.co.uk/journals⟩.)

$TGBC_{\#}$*, where "#" is used to indicate the square grid pattern. When cooling the square grid texture of Plate 57, the planar domain texture of the SmC* phase is observed to appear (Plate 58). In the texture of Plate 57 the TGB helix axis is oriented parallel to the direction of light propagation. This implies that the SmC* helix axis lies in the plane of the substrate. To obtain a square grid pattern due to the intrinsic SmC* twist, the helix axes of consecutive smectic grains also have to be perpendicular. Plate 59 [34] depicts the $TGBC_{\#}$* phase prepared in a wedge cell. Here one can clearly see the TGB helical superstructure (twist axis perpendicular to the substrate) by the appearance of Grandjean steps superimposed by a two dimensional director modulation (square grid) in the plane of the substrate, presumably due to the SmC* pitch. Pramod et al. [35] have proposed a two dimensionally undulated structure shown in Fig. 6.14 to explain the square grid texture and called this the undulated twist grain boundary C* (UTGBC*) phase. At this point it is not clear what the structural differences and similarities between $TGBC_{\#}$* and UTGBC* really are, and we cannot conclusively decide which model actually accounts for the occurrence of the square grid pattern. In any case, the TGBC* phase exhibiting the square grid texture must be a three dimensionally modulated phase.

6.3 The $TGBC_A$* Phase

Very recently, the first experimental example of a presumably *antiferroelectric* twist grain boundary phase, named $TGBC_A$*, was reported [36, 37]. The difference in smectic grain structure as compared to TGBA* and $TGBC_3$* was illustrated by switching experiments and a structure with a locally anticlinic order was proposed, as depicted in Fig. 6.15. A more detailed microscopic structural model of the director configuration in the vicinity of a grain boundary was discussed in Ref. [38], based on texture studies for applied electric fields (Fig. 6.16). To confirm this model, further experimental work will be needed in the future.

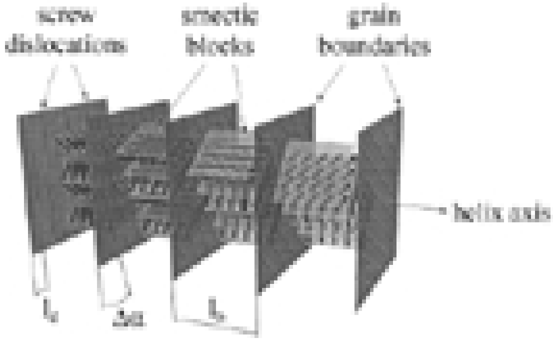

Fig. 6.15. Proposed model structure of the TGBC$_A$* phase. (Reproduced by permission of Taylor & Francis, J. G. Meier et al. *Liq. Cryst.* **29**, (2002), 179 ⟨http://www.tandf.co.uk/journals⟩.)

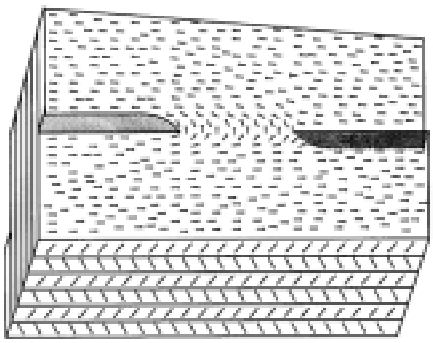

Fig. 6.16. Proposed director configuration around screw dislocations in the vicinity of a grain boundary of a TGBC$_A$* phase. (Reproduced by permission of Taylor & Francis, J. G. Meier et al. *Liq. Cryst.* **29**, (2002), 179 ⟨http://www.tandf.co.uk/journals⟩.)

References

[1] S. R. Renn, T. C. Lubensky, *Phys. Rev. A*, **38**, (1988), 132.
[2] P. G. de Gennes, *Solid State Commun.*, **10**, (1972), 753.
[3] S. R. Renn, T. C. Lubensky, *Mol. Cryst. Liq. Cryst.*, **209**, (1991), 349.
[4] W. Meissner, R. Ochsenfeld, *Naturwissenschaften*, **21**, (1933), 787.
[5] A. A. Abrikosov, *Sov. Phys. JETP*, **5**, (1957), 1174.
[6] F. London, H. London, *Proc. R. Soc. A*, **149**, (1935), 72.
[7] T. C. Lubensky, *Physica A*, **220**, (1995), 99.
[8] J. W. Goodby, M. A. Waugh, S. M. Stein, E. Chin, R. Pindak, J. S. Patel, *Nature*, **337**, (1989), 449.
[9] J. W. Goodby, M. A. Waugh, S. M. Stein, E. Chin, R. Pindak, J. S. Patel, *J. Am. Chem. Soc.*, **111**, (1989), 8119.
[10] K. Ihn, J. A. N. Zasadzinski, R. Pindak, A. J. Slaney, J. W. Goodby, *Science*, **258**, (1992), 275.
[11] L. Navailles, P. Barois, H. T. Nguyen, *Phys. Rev. Lett.*, **71**, (1993), 545.
[12] G. Srajer, R. Pindak, M. A. Waugh, J. W. Goodby, *Phys. Rev. Lett.*, **64**, (1990), 1545.
[13] F. Hardouin, M. F. Achard, J.-I. Jin, J.-W. Shin, Y.-K. Yun, *J. Phys. II*, **4**, (1994), 627.
[14] Y. Galerne, *J. Phys. II*, **4**, (1994), 1699.
[15] L. Navailles, B. Pansu, L. Gorre-Talini, H. T. Nguyen, *Phys. Rev. Lett.*, **81**, (1998), 4168.
[16] I. Dierking, S. T. Lagerwall, *Liq. Cryst.*, **26**, (1999), 83.
[17] I. Dierking, F. Giesselmann, P. Zugenmaier, *Liq. Cryst.*, **17**, (1994), 17.
[18] W. Kuczynski, H. Stegemeyer, *Ber. Bunsenges. Phys. Chem.*, **98**, (1994), 1322.
[19] W. Kuczynski, H. Stegemeyer, *Mol. Cryst. Liq. Cryst.*, **260**, (1995), 377.
[20] S. R. Renn, *Phys. Rev. A*, **45**, (1992), 953.
[21] H. T. Nguyen, A. Bouchta, L. Navailles, P. Barois, N. Isaert, R. J. Twieg, A. Maaroufi, C. Destrade, *J. Phys. II*, **2**, (1992), 1889.
[22] I. Luk'yanchuk, *Phys. Rev. E*, **57**, (1998), 574.
[23] I. Dozov, G. Durand, *Europhys. Lett.*, **28**, (1994), 25.
[24] I. Dozov, *Phys. Rev. Lett.*, **74**, (1995), 4245.
[25] L. Navailles, R. Pindak, P. Barois, H. T. Nguyen, *Phys. Rev. Lett.*, **74**, (1995), 5224.
[26] C. Destrade, S. Payan, P. Cluzeau, H. T. Nguyen, *Liq. Cryst.*, **17**, (1994), 291.
[27] M. Petit, M. Nobili, P. Barois, *Eur. Phys. J. B*, **6**, (1998), 341.
[28] R. Shao, J. Pang, N. A. Clark, J. A. Rego, D. M. Walba, *Ferroelectrics*, **147**, (1993), 255.
[29] M. Petit, P. Barois, H. T. Nguyen, *Europhys. Lett.*, **36**, (1996), 185.
[30] P. Barois, M. Nobili, M. Petit, *Mol. Cryst. Liq. Cryst.*, **302**, (1997), 215.
[31] W. Kuczynski, H. Stegemeyer, *SPIE*, **3318**, (1997), 90.
[32] W. Kuczynski, in *Selforganization in Chiral Liquid Crystals*, W. Kuczynski (ed.), Scientific Publishers OWN, Poznan, 1997.
[33] I. Dierking, *Liq. Cryst.*, **28**, (2001), 165.

[34] G. G. Nair, S. K. Prasad, D. S. Shankar Rao, C. V. Yelamaggad, *8th Int. Conf. on Ferroelectric Liquid Crystals*, Washington, DC, 2001, poster P1-43.

[35] P. A. Pramod, R. Pratibha, N. V. Madhusudana, *Curr. Sci.*, **73**, (1997), 761.

[36] J. W. Goodby, A. Petrenko, M. Hird, R. A. Lewis, J. Meier, J. C. Jones, *Chem. Commun.*, **13**, (2000), 1149.

[37] A. S. Petrenko, M. Hird, R. A. Lewis, J. G. Meier, J. C. Jones, J. W. Goodby, *J. Phys.: Condens. Matter*, **12**, (2000), 8577.

[38] J. G. Meier, P. Rudquist, A. S. Petrenko, J. W. Goodby, S. T. Lagerwall, in preparation.

Color Plates

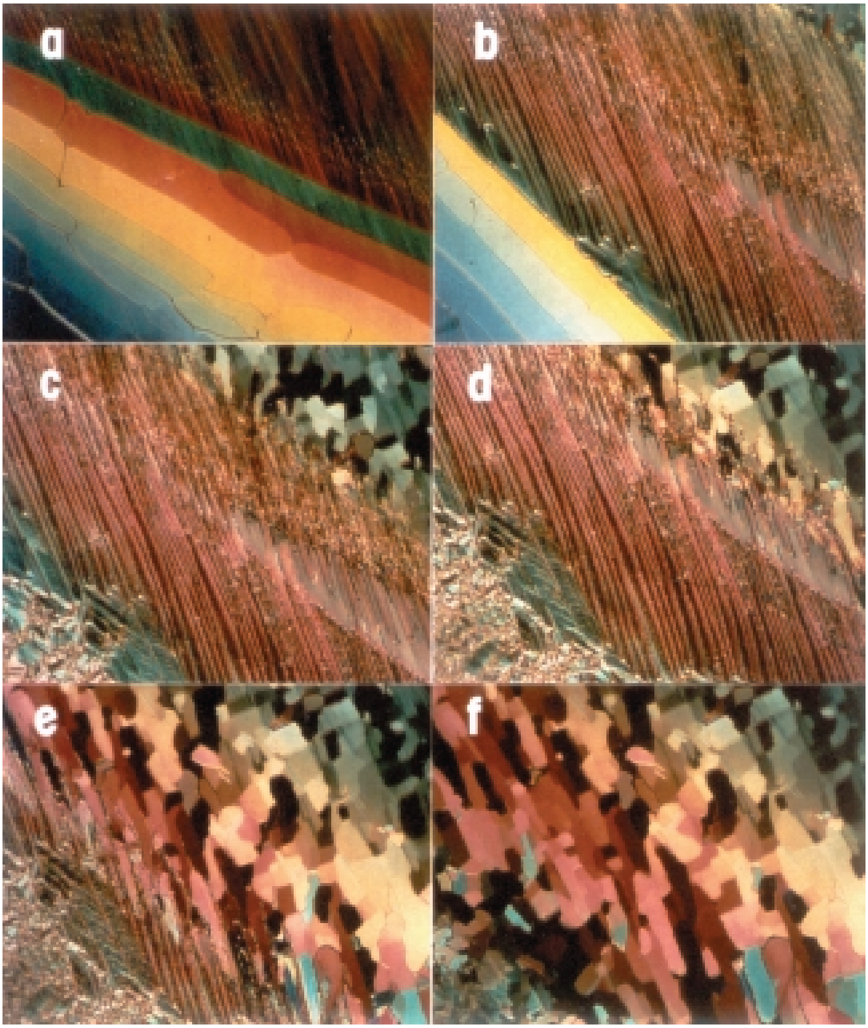

Plate 1. Example of a contact preparation for phase identification.

Plate 7. A “smectic” blue phase.

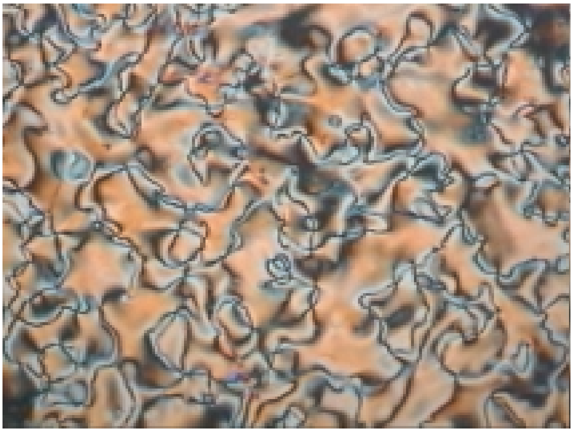

Plate 8. Schlieren texture of a nematic phase.

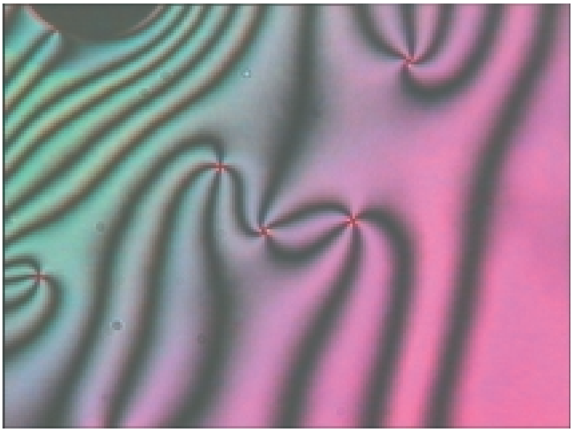

Plate 9. Schlieren texture of a nematic phase.

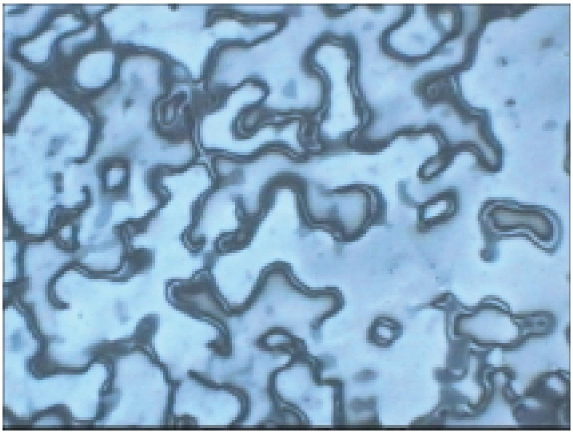

Plate 13. Nematic thread-like texture.

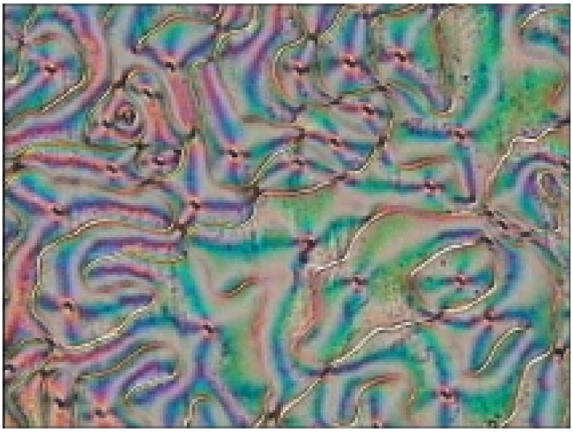

Plate 14. Nematic texture with surface disclination lines.

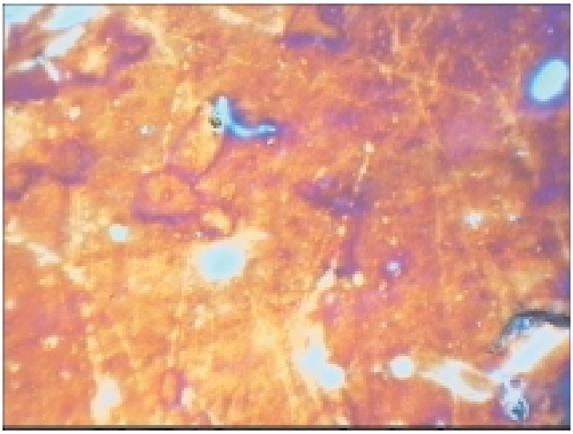

Plate 15. Nematic marble texture.